Current oscillation in superlattices with different miniband widths

E. Schomburg,* T. Blomeier, K. Hofbeck, J. Grenzer, S. Brandl, I. Lingott, A. A. Ignatov, and K. F. Renk
Institut für Angewandte Physik, Universität Regensburg, Universitätsstrasse 31, D-93040 Regensburg, Germany

D. G. Pavel'ev and Yu. Koschurinov
Department of Radiophysics, Nizhny Novgorod State University, Nizhny Novgorod, Russia

B. Ya. Melzer, V. M. Ustinov, S. V. Ivanov, A. Zhukov, and P. S. Kop'ev
A.F. Ioffe-Physico-Technical Institute, St. Petersburg, Russia

(Received 5 January 1998)

We report on current oscillation at microwave frequencies in *n*-doped wide-miniband GaAs/AlAs superlattices. We found that, with increasing miniband width (16–72 meV), the oscillation frequency increased (from 2 to 53 GHz). An analysis of the current transport, making use of the continuity and Poisson equation, indicates that the current oscillation was due to propagating dipole domains and that the oscillation frequency corresponded to the transit frequency of the domains. [S0163-1829(98)02931-2]

In recent years it has been demonstrated that doped Esaki-Tsu superlattices[1] can exhibit negative differential conductance[2] and that undoped superlattices can show photoexcited damped current oscillation.[3] Recently, a high-frequency self-sustained current oscillation at 6 GHz in a wide-miniband superlattice (miniband width 50 meV) was observed;[4] the oscillation frequency corresponded to the transit frequency expected for traveling dipole domains. It was predicted earlier[5] that, in materials (such as wide-miniband superlattices), in which electrons experience Bragg reflection, dipole domains can occur. In this paper we report on self-sustained current oscillation in doped wide-miniband GaAs/AlAs superlattices (at room temperature) with different miniband widths.

We prepared, by molecular-beam epitaxy, superlattices with different miniband widths (Table I) by choosing different well (GaAs) and barrier (AlAs) thicknesses. The width of the lowest electron miniband was calculated with a Kronig-Penney model.[6] The superlattices were of almost equal length ($L \sim 0.6\ \mu$m), with one superlattice being much shorter (0.45 μm). The superlattices were uniformly doped with Si (10^{17} cm^{-3}) and laterally structured into mesa elements (typical mesa area $10 \times 10\ \mu$m^2).

For the study of the self-sustained current oscillation, we used a broadband (100 MHz–67 GHz) measurement circuit. One mesa element of each superlattice was connected with a 50-Ω coaxial transition line with a high-frequency probe needle (picoprobe 67 A). Via the probe, a constant voltage in the range of negative differential conductance was applied to the mesa element resulting in a direct and an oscillating current. The oscillating current excited an electromagnetic wave, which was guided by the coaxial cable to a spectrum analyzing system (Tektronix 2782, with different mixers), where the spectra of the HF (high-frequency) current oscillation were registered. The HF circuit and dc circuit were separated by a bias tee.

Current-voltage (I-V) characteristics of the superlattices with different miniband widths and equal lengths are shown in Fig. 1. The I-V characteristics were antisymmetric, showing Ohmic behavior for small voltages and a negative differential conductance at larger voltages. In the region of negative differential conductance at positive voltages (ground on the top contact), current jumps appeared indicating space charge instabilities. The voltages at which the current jumps occurred and their heights were different for the different superlattices. For negative voltages (ground on the substrate), we found after the current maximum a region of negative differential conductance with a smooth slope; current oscillations did not occur. We attribute the asymmetry to a geometric asymmetry of the mesa elements having, as suggested from Ref. 7, a conuslike shape rather than a cylindrical form due to under etching.

From the peak current we obtained a peak drift velocity v_p (Table I), which increased for our superlattices by a factor of 21 when the miniband width increased by a factor of 4.6 (from 2×10^5 cm/s, for a 16-meV miniband width superlattice, up to 41×10^5 cm/s for a 72-meV superlattice). The dependence suggests that the transport in our superlattices was mainly carried by electrons in the lowest miniband. The strength of the electric field in the superlattices at the critical voltage V_c, i.e., the voltage of maximum current, was almost

TABLE I. Structural data and experimental results of our superlattices.

Δ (meV)	Well (Å)	Barrier (Å)	Length (μm)	Doping (10^{17} cm^{-3})	v_p (10^5 cm/s)	$\nu_{\rm osc}$ (GHz)
16	31.0	19.6	0.55	0.8	2	2
22	48.6	13.0	0.74	1.3	9	9
43	51.3	8.7	0.60	1.4	20	20
46	48.0	9.0	0.57	0.8	27	29
55	40.0	10.0	0.5	0.8	31	46
72	36.4	9.3	0.64	1.0	41	53
72	35.4	9.6	0.45	0.9	34	65

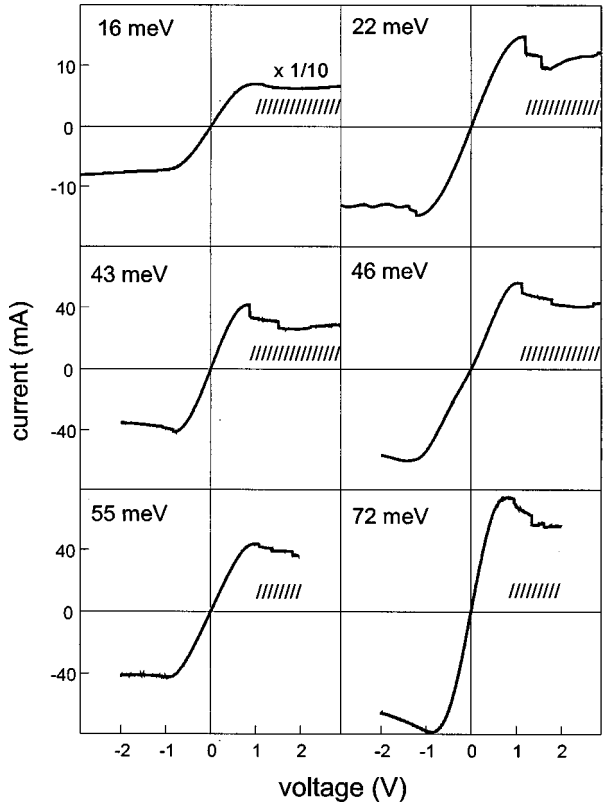

FIG. 1. *I-V* characteristics of superlattices with different miniband widths; dashed lines indicate regions of current oscillation.

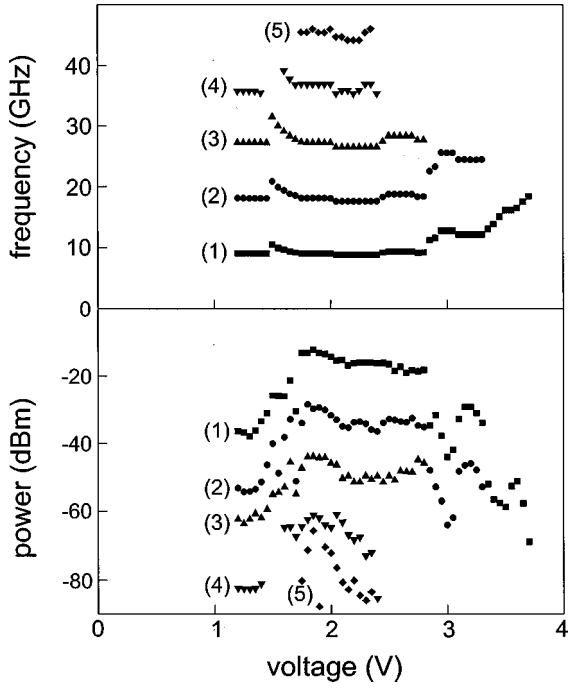

FIG. 2. Voltage dependence of the frequencies (a) and the power (b) of the harmonics of the 22-meV superlattice.

independent of the miniband width, and had a value of ~14 kV/cm.

We observed current oscillation in our superlattices in the region of negative differential conductance at positive voltages (dashed regions in Fig. 1). The voltage dependence of the harmonics of the current oscillation for the 22-meV superlattice is shown in Fig. 2. We observed current oscillation right after the first current step in a range between 1.2 and 3.7 V. At voltages between 1.2 and 2.8 V, the oscillation frequency ν_{osc} was almost constant at 9 GHz and up to four higher harmonics occurred. At higher voltages the oscillation frequency increased (up to 18 GHz at 3.7 V) and the number of harmonics decreased. The HF power of the fundamental and the first two higher harmonics changed within a factor of 3 in a wide voltage range (1.7–2.8 V); beyond this range the power was significantly smaller. We found that the oscillation frequency and the HF power changed abruptly at voltages, where current steps occurred, while in smooth parts of

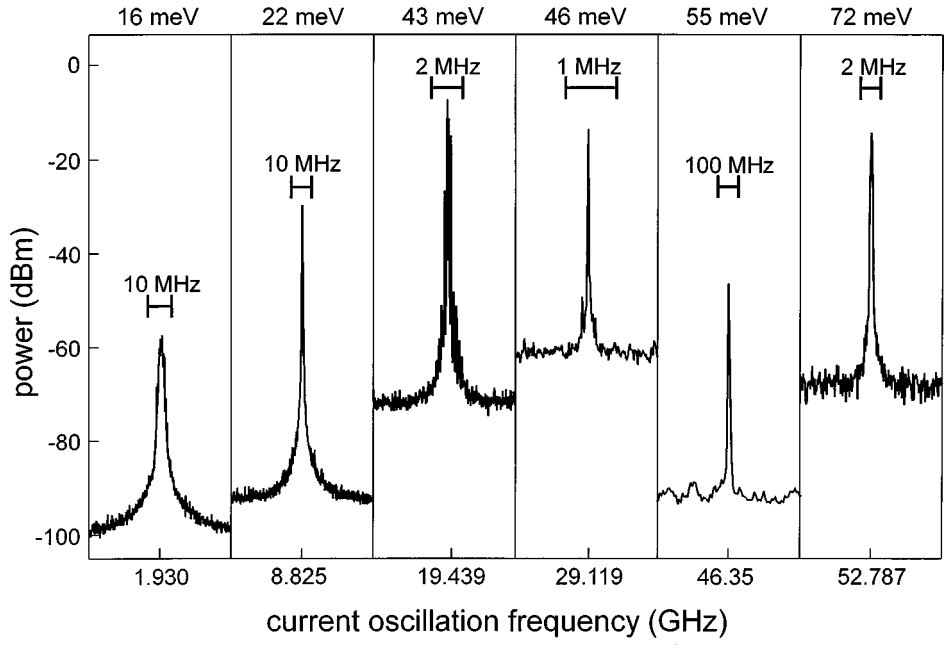

FIG. 3. Fundamental harmonics of the current oscillation of superlattices with different miniband widths and almost equal length.

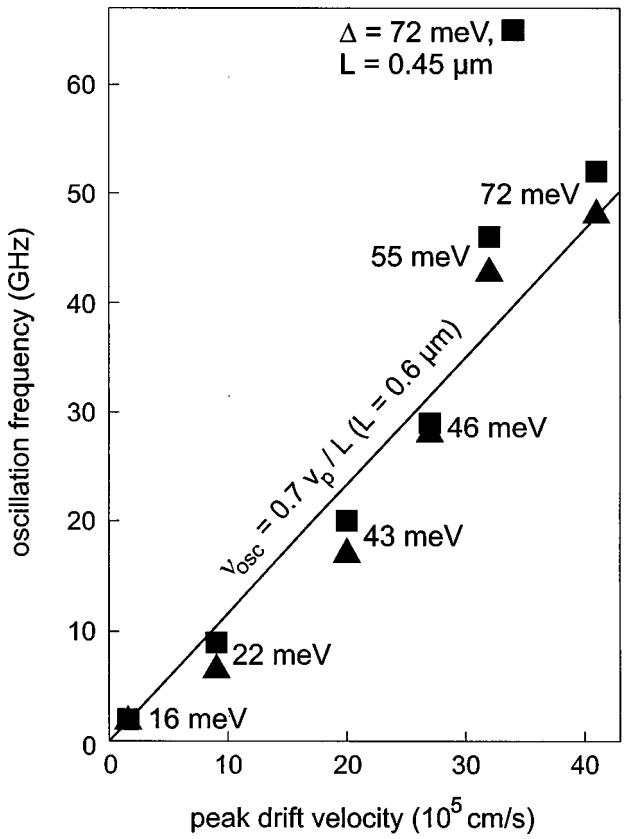

FIG. 4. Current oscillation frequencies for superlattices with different peak drift velocities (squares, experiment; triangles, simulation).

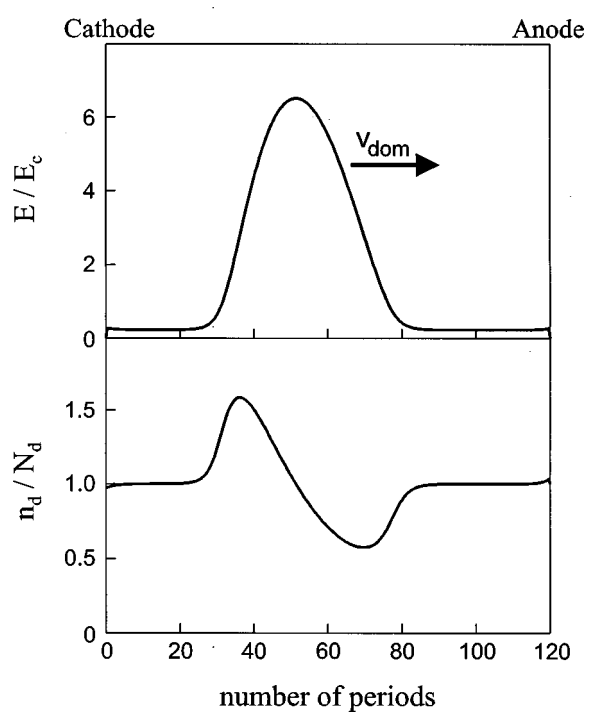

FIG. 5. Traveling dipole domain in the 22-meV superlattice, with the field distribution (upper curve) and the carrier distribution (lower curve) propagating with the domain velocity v_{dom}.

the current-voltage characteristic the oscillation frequency and the HF power were almost constant or changed continuously.

The spectra of the fundamental harmonics for different superlattices biased at the same voltage related to the critical voltage ($\sim 2V_c$) are shown in Fig. 3. We found that with increasing miniband width the oscillation frequency increased (from 2 GHz for the 16-meV superlattice up to 53 GHz for the 72-meV superlattice). The highest HF power of 500 μW with a conversion from dc to HF power of $\sim$1% was observed for the 43-meV superlattice at an oscillation frequency of 20 GHz. The fundamental harmonics of the superlattices showed different line widths (full width at half-maximum) in the range from about 3 MHz (16-meV superlattice) up to less than 10 kHz (46-meV superlattice). At present, we have no explanation for the different linewidths.

In Fig. 4 we plotted the experimental data (squares) of the oscillation frequency, ν_{osc}, versus the peak drift velocity. The straight line, calculated by the ratio $\nu_{\mathrm{osc}}=0.7\, v_p/L$ ($L=0.6\,\mu$m), described well the dependence of our experimental data. For the 72-meV superlattices with different length, we found that a decrease of the length led to an increase of the oscillation frequency (from 53 to 65 GHz), although the shorter superlattice had a slightly smaller peak drift velocity than the longer one. From our results, we conclude that the oscillation frequency strongly depends on the peak drift velocity and the length of the superlattice.

For an analysis of our experimental results, we compared the peak drift velocity of the superlattice with a calculation using a semiclassical model,[8] which takes into account inelastic and elastic intraminiband relaxation,

$$v_p=\frac{\Delta a}{4\hbar}\,\frac{I_1\left(\frac{\Delta}{2kT}\right)}{I_0\left(\frac{\Delta}{2kT}\right)}\left(\frac{\nu_\varepsilon}{\nu_\varepsilon+\nu_{\mathrm{el}}}\right)^{(1/2)}, \tag{1}$$

where a is the superlattice period, Δ the miniband width, I_1 and I_0 the first and second modified Bessel function, ν_ε the inelastic scattering rate, ν_{el} the elastic scattering rate, T temperature, k Boltzmann's constant, and $\hbar$ Planck's constant. The ratio of the modified Bessel functions describes a reduction of the drift velocity due to a thermal distribution of the miniband electrons at the temperature T.[9] Elastic scattering, caused by the roughness of the superlattice interfaces or defects, also leads to a reduction of the drift velocity, described by the last factor of Eq. (1).[8] Our calculation ($T=300$ K) delivers a good agreement with the experimental peak drift velocities (Table I) of our superlattices for $\nu_\varepsilon/(\nu_\varepsilon+\nu_{\mathrm{el}})\sim 0.25$. A similar value was reported for undoped superlattices studied by time-of-flight measurements.[10] Taking into account the critical voltage[8] $V_c=(\hbar/e)N\nu_\varepsilon^{1/2}(\nu_\varepsilon+\nu_{\mathrm{el}})^{1/2}$, where N is the number of superlattice periods and e the elementary charge, we estimated the elastic (2×10^{13} s^{-1}) and the inelastic (9×10^{12} s^{-1}) scattering rate. We suggest that the inelastic scattering in the superlattices at room temperature was due to interaction with optical phonons.[11,12] Different peak drift velocities for the 72-meV superlattices (Fig. 4, Table I) were probably due to different elastic scattering rates caused by different qualities of the interfaces between GaAs and AlAs layers.

We simulated the current through the superlattices with a model, which has been earlier developed for Gunn devices.[13] Our analysis included a self-consistent calculation of the one-dimensional Poisson equation $\partial E/\partial z=(e/\varepsilon_0\varepsilon)(n_d-N_d)$ and the time dependent continuity equation $\partial(n_d-N_d)/\partial t=-(1/e)(\partial j/\partial z)$, where E is the electric field, z the direction along the superlattics axis, ε_0 the electric-field constant, ε the dielectric constant of the superlattice material, n_d the charge density, N_d the doping level, $j=en_dv_D-e\partial(Dn_d)/\partial z$ the current density and t the time. We assumed that the local transport properties were determined by a velocity-field characteristic $v_D=2v_pE/\{E_c[1+(E/E_c)^2]\}$ and a field-independent diffusion term D, calculated from the Einstein relation $D=(kT/e)\mu$, where $E_c=V_c/L$ is the field at the onset of negative differential conductance, and $\mu=2v_p/E_c$ is the low-field mobility. We used the doping level, the length of the superlattice, and the values v_p and V_c, taken from the I-V characteristics, as input parameters for the simulation of the evolution of the carrier density inside the superlattice. For the calculation, we assumed that a constant voltage V was applied to the superlattice, with the condition $V=\int_0^L E dz$.

For voltages larger than V_c, the simulation showed the formation of a traveling dipole domain. After the build up of a domain, a stationary state appeared, where the traveling domain kept the shape constant due to a dynamical equilibrium between drift and diffusion processes. The velocity of the domain v_{dom} depended on the field outside the domain; v_{dom} was smaller than the peak drift velocity. At the anode the dipole domain was quenched, causing a current spike in the external circuit, and another domain appeared at the cathode. The process of domain formation and quenching was repeated periodically leading to a current oscillation at a transit frequency equal to the domain velocity divided by the superlattice length ($\nu_{\mathrm{osc}}=v_{\mathrm{dom}}/L$). We found that the transit frequency almost corresponded to the experimental oscillation frequency ν_{osc} (Fig. 4: squares, experiment; triangles, simulation). The estimated domain velocity for the superlattices biased at $2V_c$ was about $0.7v_p$. The appearance of domains resulted also in a jump and a decrease of the direct current as observed in the I-V characteristics (Fig. 1).

Figure 5 shows results of the calculation of the spatial field and carrier distribution inside the 22-meV superlattice at a voltage of $2V_c$. The carrier distribution has the shape of a dipole domain with a depletion layer followed by an accumulation layer. Corresponding to the carrier distribution, the electric field inside the superlattice is splitted in a high-field region (with a value up to $6E_c$) and a low-field region. The width of a domain is about a third of the superlattice length. This is consistent with the observation of higher harmonics (Fig. 2). A similar field and carrier distribution was also found for the other superlattices.

With a total high-frequency power of about 500 μW (43-meV superlattice), a superlattice may be suitable for a low-power oscillator. We suggest that the oscillation frequency of this superlattice oscillator can be chosen by an appropriate choice of the GaAs and AlAs layer thickness, and the length of the superlattice.

In conclusion, we showed that the current oscillation frequency in superlattices with different miniband widths increased proportionally to the peak drift velocity, which strongly depends on the miniband width. A decrease of the superlattice length leads to an increase of the oscillation frequency. A numerical analysis based on a local velocity-field characteristic and a field-independent diffusion term showed that the current oscillation was due to traveling dipole domains and that the oscillation frequency corresponded to the transit frequency of the domains.

We would like to acknowledge fruitful discussions with A. Wacker, G. Schwarz, and E. Schöll.

*Electronic address:
ekkehard.schomburg@physik.uni-regensburg.de

[1] L. Esaki and R. Tsu, IBM J. Res. Dev. **14**, 61 (1970).
[2] A. Sibille, J. F. Palmier, H. Wang, and F. Mollot, Phys. Rev. B **39**, 6272 (1989); M. Hadjazi, A. Sibille, J. F. Palmier, and F. Mollot, Electron. Lett. **27**, 1101 (1991).
[3] H. Le Person, C. Minot, L. Boni, J. F. Palmier, and F. Mollot, Appl. Phys. Lett. **60**, 2397 (1992).
[4] K. Hofbeck, J. Grenzer, E. Schomburg, A. A. Ignatov, K. F. Renk, D. G. Pavel'ev, Yu. Koschurinov, B. Melzer, S. Ivanov, S. Schaposchnikov, and P. S. Kop'ev, Phys. Lett. A **218**, 349 (1996).
[5] M. Büttiker and H. Thomas, Phys. Rev. Lett. **38**, 78 (1977).
[6] G. Bastard, Phys. Rev. B **24**, 5693 (1981).
[7] E. Schomburg, J. Grenzer, K. Hofbeck, C. Dummer, S. F. Winnerl, A. A. Ignatov, K. F. Renk, D. G. Pavel'ev, Yu. I. Koschurinov, B. Melzer, S. Ivanov, V. Ustinov, and P. S. Kop'ev, IEEE J. Sel. Top. Quantum Electron. **2**, 724 (1996).
[8] A. A. Ignatov, E. P. Dodin, and V. I. Shashkin, Mod. Phys. Lett. B **5**, 1087 (1991); A. A. Ignatov, E. Schomburg, J. Grenzer, K. F. Renk, and E. P. Dodin, Z. Phys. B **98**, 187 (1995).
[9] G. Brozak, M. Helm, F. DeRosa, C. H. Perry, M. Koza, R. Bhat, and S. J. Allen, Phys. Rev. Lett. **64**, 3163 (1990).
[10] C. Minot, H. LePerson, J. F. Palmier, and F. Mollot, Phys. Rev. B **47**, 10 024 (1993).
[11] B. Goutiers, F. Aristone, E. Ranz, and F. Mollot, Superlattices Microstruct. **17**, 135 (1995).
[12] S. Winnerl, E. Schomburg, J. Grenzer, H.-J. Regl, A. A. Ignatov, A. D. Semenov, K. F. Renk, D. G. Pavel'ev, Yu. Koschurinov, B. Melzer, V. Ustinov, S. Ivanov, S. Schaposchnikov, and P. S. Kop'ev, Phys. Rev. B **56**, 10 303 (1997).
[13] P. Jeppesen and B. I. Jeppsson, IEEE Trans. Electron Devices **ED-18**, 439 (1971).